Computer Modeling in Engineering & Sciences CMES, vol.122, no.3, pp.1055-1080, 2020

Dimensionless Variation of Seepage in Porous Media with Cracks Stimulated by Low-Frequency Vibration

Liming Zheng[1, 3, *], Xiaodong Han[2, 4], Xinjun Yang[1], Qingzhong Chu[1] and Guanghui Li[1]

Abstract: Pulse excitation or vibration stimulation was imposed on the low permeable formation with cracks to enhance the production or injection capacity. During that process, a coupling of wave-induced flow and initial flow in dual-porous media was involved. Researchers had done much work on the rule of wave propagation in fractured porous media, whereas attentions on the variation law of flow in developing low permeable formation with cracks under vibration stimulation were not paid. In this study, the effect of low-frequency vibration on the seepage in dual-porous media was examined for the application of wave stimulation technology in developing reservoirs with natural cracks. A model for seepage of single-phase liquid in porous media with cracks under low-frequency vibration excitation was built by combining wave propagating theory for porous media with cracks and dual-porous media seepage mechanics. A governing equation group for the model, which was expressed by dimensionless fluid and solid displacements, was derived and solved with a numerical method. Variable physical properties were simulated to check the applicability of external low-frequency vibration load on dual-porous media and a parametric study for various vibration parameters. Stimulation of low-frequency vibration affected flow velocities of crack and rock matrix fluids. Compared with that in single-porous media, the stimulation effect on the fluid inner matrix of dual-porous media was relatively weakened. Different optimal vibration parameters were needed to increase the channeling flow between the crack and rock matrix or to only promote the flow velocity in the rock matrix. The theoretical study examines wave-coupled seepage field in fractured porous media with results that are applicable for low-frequency stimulation technology.

Keywords: Low-frequency vibration, wave-induced flow, dual-porous media, crack, dimensionless.

[1] College of Vehicles and Energy in Yanshan University, Qinhuangdao, China.

[2] Institute of Unconventional Oil and Gas Science and Technology, China University of Petroleum, Beijing, China.

[3] Mechanical Engineering Postdoctoral Station in Yanshan University, Qinhuangdao, China.

[4] China National Offshore Oil Corporation China Ltd., Tianjin Branch, Tianjin, China.

[*] Corresponding Author: Liming Zheng. Email: upczlm@sina.cn.

Received: 09 June 2019; Accepted: 28 October 2019.

1 Introduction

Pulse excitation or vibration stimulation was an important method to promote fluid flow in porous media in rock mechanics or energy development field [Saiood, Duthie, Shaheen et al. (2018); Zheng and Li (2018)]. Wave-induced flow like Biot flow or squirt flow occurs in micro-pores [Biot (1956); Dvorkin, Mavko and Nur (1995)]. Because of the heterogeneity and micro-damage of natural rock, the wave-induced flow would be influenced by the existence of micro-cracks. Wave propagation theory in fractured porous media was investigated in petrophysics. Several theories including the Hudson, Thomsen, and Chapman models described the constitutive relation or the modulus in fractured porous media under vibration [Hudson, Pointer and Liu (2001); Berryman (2007); Chapman (2009)]. The theories had mainly focused on the wave propagation rule. The crack was interconnected or isolated, and the fluid was assumed static at the initial time.

For the cases with vibration stimulation in developing reservoirs with cracks [Tian, Huang, Li et al. (2018)], fluid flow can be divided into two parts, one caused by injection-production pressure difference at the initial time, and the other one being wave-induced flow. The coupling of two kinds of fluid flow should be considered, and the coupled flow was named wave-coupled seepage [Pu, Zheng and Liu (2017)]. Low-frequency vibration oil production technology, which was also called the artificial seismic technology, had been applied in reservoirs with cracks and was connected with the wave-coupled seepage. Other cases could be found in pulse fracturing technology and electrical impulse stimulation technology [Zhang, Huang, Li et al. (2018); Ma (2019)]. It was helpful to study the variation of seepage in reservoirs with cracks under vibration stimulation conditions so as to investigate the action mechanism of above technologies. It could also present that whether it was effective and what vibration parameters should be chosen, when these technologies were applied in dual-porous media.

Theoretical research on wave fields in porous media with cracks was mostly related to elastic wave propagation in fractured porous media. The rule of fracture extension under pulsating excitation was also studied through experiments and numerical analysis. Several studies examined the variation of wave propagation rule or fracture extension [Ning, Ning, Shi et al. (2014); Alexandre, Philip, Ben et al. (2006); Mosaheb, Zeidouni and Shakiba (2018); He, Xiong, Lu et al. (2018)], while the variation of the flow field in the whole dual-porous media was not often studied. So, the variation of seepage was most commonly studied. There have been a limited number of studies on the influence of low-frequency wave vibration on the seepage field of fractured porous media. A few field trials or experiments on using the artificial seismic technology in fractured reservoirs were published [Zhang (2011); Wang, Xie, Gao et al. (2016)]. Theoretical research with mathematical model building and numerical analysis is needed to improve understanding of these topics.

Wave propagation theory for fractured porous media must be combined with the theory of seepage mechanics of dual-porous media to effectively simulate variation of seepage in porous media with cracks stimulated by low-frequency vibration. The former theory took into account the effect of wave-induced flow and the variation of effective stiffness under matrix pulsating excitation, but merely considered the initial flow in the pores. The latter theory showed enhanced flow under vibration or pulsation, but wave-induced flow was

not introduced [Warrant and Root (1963); Fang and Jin (2007); Wu, Zhang, Cao et al. (2016)]. Initial fluid flow and wave-induced flow in single-porous media were coupled [Zheng, Liu, Pu et al. (2016); Zheng, Pu and Liu (2018)], but in this study, initial fluid flow and wave-induced flow are combined in a dual porous media. This approach connects petrophysics and seepage mechanics despite their differences regarding assumption on the shape of crack, whether physical properties change with time and position, or the definite conditions.

Firstly, the parameters describing crack properties (simplified into crack parameters below) in two theories were characterized, and an equivalent relationship was established. Then, a mathematic model was given to describe the seepage in porous media with cracks under low-frequency vibration excitation. A governing equation group of the mathematical model was derived and expressed by dimensionless fluid and solid displacements. Finally, the variation of physical properties in wave-coupled seepage field was numerically simulated. The influence of vibration parameters and heterogeneity on physical properties of dual-porous media was made through sensitivity analysis.

2 Mathematic model

2.1 Model assumptions

The difference between hypotheses should be made clear before establishing the mathematical model. The seepage model of dual-porous media usually assumes a high crack or fracture density. For the Warren-Root model, one of the most classical seepage models of dual-porous media, the crack density was high enough and the pressure in a matrix cell was about the same [Warrant and Root (1963)]. Channeling of flow between the crack and matrix pore was only related to the difference of their pressures. Wave propagation theory in fractured porous media was usually assumed to have a low crack or fracture density [Vladimir (2014)]. It was essential to choose a wave propagation model with proper crack density so as to assume that it is adaptable to a seepage model of dual-porous media. Compared with the Hudson model, the Chapman model accounted for the existence of fractures and cracks. Interconnection between the isolated fractures can be achieved through the cracks [Chapman (2003, 2009)]. The Chapman model described the mesoscale fluid flow between fractures and cracks or spherical pores. It also described the particle-scale fluid flow between micro-cracks and spherical pores or the particle-scale fluid flow between different spherical pores. When the densities of fractures and cracks in the Chapman model was relatively high, a physical network was approximated as a porous media with interconnected fractures, just as that of the Warren-Root model, which was not evenly distributed.

To some extent, a connection between two theories was made, thereby, on the premise of additional assumptions. (1) densities of fractures and cracks in wave propagation theory were set to the upper limit, and (2) the shapes of fracture and crack were same, so they could be classified into one kind of pore structure. A coupling of Chapman model and Warren-Root model were made to simplify the theoretical analysis. The assumption was suitable for the area nearby the injection well in low permeable reservoirs with evenly distributed cracks, and the reservoirs were not large scale hydraulic fractured (for example the shallow low permeable oil field in Ordos basin). It was also suitable for deep

area in the fractured formation, where wave stimulation was still effective.

Except for above assumptions, other traditional conditions were also introduced, on the basis of the background of wave stimulation technology and wave propagation theory in fractured porous media [Dusseault, Davidson and Spanos (2000); Karve, Kallivokas and Manuel (2017)]. (1) The rock was homogeneous, elastic, and isotropic sandstone, cracks were evenly distributed in the rock, and the matrix pores and cracks were saturated with a single-phase compressible liquid. (2) The constitutive relationship of rock influenced by low-frequency vibration oil production technology conformed to that of wave propagation theory of fractured porous media. (3) The strain of porous media only considered that of skeleton, ignoring the strain of solid particles and the damage of crack by wave-induced flow. (4) Biot flow and squirt flow occurred in the matrix pore under vibration, whereas a slight Biot flow was caused in the crack that had high conductivity. (5) At the initial time, the flowing liquid in the rock was influenced by injection-production pressure difference and pseudo-threshold pressure gradient, instead of vibration. (6) A low-frequency source wave was excited, its wavelength was much longer than the average pore-throat length, and no thermal effect was caused by the low-frequency vibration.

2.2 Equivalent relationship for crack parameters

At present, the seepage mechanics of dual-porous media and the elastic wave propagation theory of fractured porous media are studied independently in the oil-gas development engineering field. The crack parameters used by the two theories were different (Fig. 1). The former usually included aperture, density length, permeability, and porosity of the crack. In the theoretical model the shape of the crack was assumed to be a line, rectangle, wedge, or cuboid. The later was usually described with aspect ratio (ratio of crack aperture to the diameter of a coin-shaped crack), density, and average radius. The shape of the crack was assumed to be a line, coin shape, circular, ellipse, or sphere. Thereby, a connection had to be made between these crack parameters to build a wave-coupled seepage model for porous media with cracks.

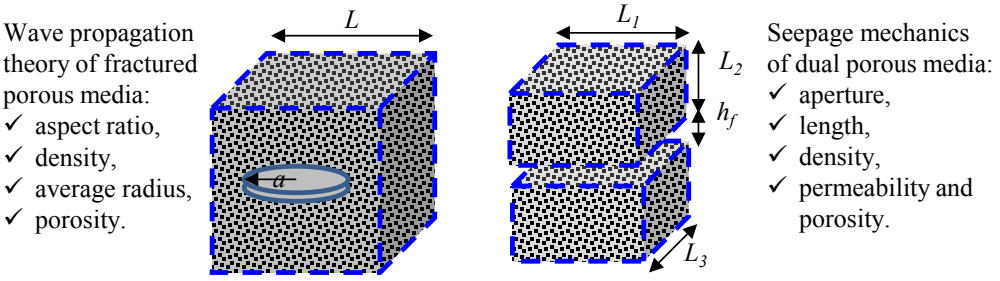

Figure 1: Crack parameters mainly used in the two basic models

The crack in petrophysics was represented using a classic coin-shape with a radius a, while the interconnected or isolated crack in seepage mechanics was with cuboid-shape, an aperture h_f, and characteristic length $L_1 \times L_2$. Referring to the definition of flow

radius in fluid mechanics, the relationship between characteristic length and average radius was given in Eq. (1).

$$\frac{1}{a}=2\left(\frac{1}{L_1}+\frac{1}{L_2}\right), \tag{1}$$

wherein a was the average radius of coin-shape crack; h_f was the crack aperture; L_1 and L_2 were the characteristic lengths of crack in seepage mechanics, $L_1 \geq L_2 >> h_f$.

When the crack was assumed two-dimensional, the characteristic length of crack equaled to the length of matrix cell, then Eq. (1) is simplified as $a = L_1 / 2$.

The relationship between fracture density and fracture porosity was shown in Eq. (2).

$$\varepsilon_f = \frac{3\phi_f}{4\pi\gamma} \text{ or } \varepsilon_f = \frac{N\overline{a}^3}{V} = \frac{N\pi a^2 h_f}{V} = f_3\overline{a}^2, \tag{2}$$

wherein $\overline{a}$ was the radius of spherical crack; ϕ_f was the crack porosity; γ was the aspect ratio of fracture and less than 0.3, $\gamma = h_f / (2a)$; V was the rock volume; N was the number of crack in volume V; f_3 was the crack density in unit volume.

The crack permeability could be described by the crack porosity and crack aperture as Eq. (3).

$$k_f = \frac{\phi_f h_f^{\,2}}{12}, \tag{3}$$

wherein k_f was the crack permeability.

2.3 Seepage model in porous media with cracks under low-frequency vibration

The stiffness tensor in the constitutive relationship of the Chapman model was introduced into the Warrenroot model, and the crack paramaters were expressed by Eqs. (1)-(3). Then, the model of seepage in porous media with cracks under low-frequency vibration was obtained by combing the constitutive relationship, motion equation, continuity equation, state equation, auxiliary equation, and definite equation.

(1) Stiffness tensor in constitutive relationship of Chapman model

The expression of the effective stiffness tensor of the Chapman model is shown in Eq. (4). Because the Chapman model was suitable for a low porosity condition, a high error might be caused in a case of high porosity when calculating the stiffness tensor with the Lamécoefficients of particles (λ and μ). Thereby, new Lamé constants (Υ and $\wedge$) was introduced in and the effective stiffness tensor of Chapman model was shown in Eq. (5) [Chapman (2003, 2009)].

$$C = C^0 - \phi_m C^1 - \varepsilon_c C^2 - \varepsilon_f C^3, \tag{4}$$

$$C(f)=C^0(\wedge,\Upsilon)-\phi_m C^1(\lambda^0,\mu^0,f)-\varepsilon_c C^2(\lambda^0,\mu^0,f)-\varepsilon_f(\lambda^0,\mu^0,f), \tag{5}$$

wherein, C was the modulus matrix of porous media with cracks under vibration; C^0 was the elastic modulus matrix of rock skeleton (or rock matrix), which could be expressed by Lamé coefficients; ϕ_m was the porosity of rock matrix; C^1, C^2, and C^3 was the additional contribution to modulus matrix from pore, micro crack and fracture, respectively, and they were related with Lamé coefficients, fluid properties, fracture properties, vibration frequency as well as relaxation time related to squirt flow; ε_c was the density of micro crack; ε_f was the density of fracture; Υ and $\wedge$ were the newly introduced Lamé constants; f was the vibraton frequency; λ^0 and μ^0 was Lamé coefficients of particles.

(2) Momentum equation considering wave-induced inertia effect

The momentum equation for wave propagation theory was expressed by continuum theory. Under the influence of low-frequency fluctuation, Biot flow, and squirt flow could be generated in the finite pore space of the rock matrix. The inertia and viscous effects on the fluid both affected the seepage in the rock matrix [Ekanem, Li, Chapman et al. (2014)]. When the wave-induced flow transferred effectively along the direction of fracture extension in the case of high porosity rock, the fluid diffusion length was longer than the characteristic size of the fracture, there was enough time to achieve a balance between the crack pressure and the pore pressure. Only a slight Biot flow occurred in the crack under low-frequency vibration. Squirt flow was ignored because of the large crack permeability. The momentum equation of solid phase, fluid in rock matrix, and fluid in crack were shown as Eq. (6) to Eq. (8):

$$\nabla\sigma^*=C\nabla e-\left(\alpha_m\phi_m\nabla P_m+\alpha_f\phi_f\nabla P_f\right)+\rho_s b^S=\rho\frac{\partial^2\sqcup u}{\partial t^2}+\rho_m\frac{\partial^2\sqcup w_m}{\partial t^2}+\rho_f\frac{\partial^2\sqcup w_f}{\partial t^2}, \tag{6}$$

$$-\nabla P_m+\rho_m b_m{}^F\approx\left[1-\frac{2J_1(\lambda_m R_m)}{\lambda_m R_m J_0(\lambda_m R_m)}\right]\left[\rho_m\left(\frac{\partial^2\sqcup u}{\partial t^2}+\frac{1}{\phi_m}\frac{\partial^2\sqcup w_m}{\partial t^2}\right)+\frac{\eta}{k_m}\frac{\partial\sqcup w_m}{\partial t}\right], \tag{7}$$

$$-\nabla P_f+\rho_f b_f{}^F\approx\rho_f\left(\frac{\partial^2\sqcup u}{\partial t^2}+\frac{1}{\phi_f}\frac{\partial^2\sqcup w_f}{\partial t^2}\right)+\frac{\eta}{k_f}\frac{\partial\sqcup w_f}{\partial t}, \tag{8}$$

wherein σ^* was the effective stress on the rock; e was the strain; u was the solid displacement; α_m and α_f was Biot coefficients of rock matrix and crack, $\alpha_m=1-\frac{K_{bm}}{K_s}$, $\alpha_f=1-\frac{K_{bf}}{K_s}$; K_s and K_{bi} (i=m, f) were the volume modulus of saturated rock and the volume modulus of rock, it was assumed $K_{bm}=K_{bf}$ in the study; P_m and P_f was the fluid pressure in rock matrix and fracture, respectively; ρ_s

was the density of rock matrix; b^S was the body force term acting on the matrix; ρ was the density of porous media, $\rho = \phi_m \rho_m + \phi_f \rho_f + \left(1-\phi_m-\phi_f\right)\rho_s$; ρ_m and ρ_f was the density of fluid in rock matrix and crack, respectively; w_m and w_f was the relative displacement of fluid in rock matrix and crack, respectively; b_i^F (i=m, f) was the body force term acting on the fluid; J_1 and J_0 were the first and zero order Bessel functions; R_m was the length of squirt flow in rock matrix; $\lambda_m R_m = \sqrt{R_m{}^2 \frac{\rho_m \omega^2}{F_1}\left(\frac{\phi_m - \rho_{12}/\rho_m}{\phi_m} + \frac{\omega_{cm}}{\omega}\right)}$; ω was the angular frequency, $\omega = 2\pi f$; ω_{cm} was the characteristic angular frequency in Biot theory , $\omega_{cm} = \frac{\eta \phi_m}{k_m \rho_m}$; $\frac{1}{F_1} = \frac{1}{K_f} + \frac{1}{\phi_m Q_1}$, $\frac{1}{Q_1} = \frac{1}{K_s}\left(\alpha_m - \phi_m\right)$; K_f was the volume modulus of fluid; Q_1 was a coefficient in Biot poroelastic theory; ρ_{12} was the coupled density, referring to the supplementary equation by Berryman [Berryman (1979)], $\rho_{12} = \left(1-\alpha_{cou}\right)\phi_m \rho_m$; α_{cou} was the tortuosity coefficient, for a case of sphere matrix particle, $\alpha_{cou} = 0.5\left(1/\phi_m + 1\right)$; k_m and k_f was the permeability of rock matrix and crack; η was the fluid viscosity.

For a low permeability reservoir, the pseudo-threshold pressure gradient should be considered during the reservoir development process [Wang, Rutqvist, Görke et al. (2011)]. Eq. (7) was rewritten as Eq. (9):

$$\begin{cases} \nabla P_m = \nabla P_m - \lambda_0, & \nabla P_m > \lambda_0 \\ \rho_m\left(\frac{\partial^2 \vec{u}}{\partial t^2} + \frac{1}{\phi_m}\frac{\partial^2 \vec{w}_m}{\partial t^2}\right) + \frac{\eta}{k_m}\frac{\partial \vec{w}_m}{\partial t} = 0, & \nabla P_m < \lambda_0 \end{cases}, \tag{9}$$

wherein λ_0 was the pseudo-threshold pressure gradient.

(3) Continuity equations of liquid phase and solid phase

The continuity equation of solid phase was represented using Eq. (10),

$$\nabla \cdot \left[\left(1-\phi_m-\phi_f\right)\rho_s \frac{\partial u}{\partial t}\right] + \frac{\partial}{\partial t}\left[\left(1-\phi_m-\phi_f\right)\rho_s\right] = 0 . \tag{10}$$

and the continuity equation of fluid in rock matrix and crack was represented using Eqs. (11) and (12),

$$\nabla \cdot \left[\rho_m \frac{\partial\left(w_m + \phi_m u\right)}{\partial t}\right] + \frac{\partial\left(\rho_m \phi_m\right)}{\partial t} + q^* = 0 , \tag{11}$$

$$\nabla \cdot \left[\rho_f \frac{\partial}{\partial t}\left(w_f + \phi_f u \right) \right] + \frac{\partial \left(\rho_f \phi_f \right)}{\partial t} - q^* + q_0 = 0, \tag{12}$$

wherein q_0 was the source or sink term, representing the injection or production rate per unit volume of underground rock; q^* was the channeling flow rate between the crack and rock matrix.

Referring to the seepage mechanics of dual-porous media, the channeling flow rate was given as Eq. (13),

$$q^* = \frac{\alpha_{shape} \rho_m k_m}{\eta} \left(P_m - P_f \right), \tag{13}$$

wherein α_{shape} was the shape factor, and Lei [Lei (2014)] found that Costs model approached the experimental result, $\alpha_{shape} = \frac{16}{L^2}$ in two dimensional situation and $\alpha_{shape} = \frac{24}{L^2}$ in three-dimensional situation; L was the average characteristic length of the matrix cell as in Eq. (1).

(4) State equation

The variation of liquid density was expressed as Eq. (14). The change of solid density was caused by strain and variation of fluid pressure as Eq. (15).

$$\frac{d\rho_m}{\rho_m} = \frac{1}{K_f} dP_m, \quad \frac{d\rho_f}{\rho_f} = \frac{1}{K_f} dP_f, \tag{14}$$

$$\left(1 - \phi_m - \phi_f \right) d\rho_s = \rho_s \left[\left(\alpha - 1 \right) de + \frac{1}{Q_c} dP \right]. \tag{15}$$

wherein, $\left(\alpha - 1 \right) de$ represented the density change term caused by matrix deformation; $\frac{1}{Q_c} dP$ represented the volume change term caused by fluid compression; α was assumed the sum of α_m and α_f; similar to the equivalent fluids used by others [Corapcioglu (1973); Mavko, Mukerji and Dvorkin (1998)], it was assumed that $\frac{1}{Q_c} dP = \frac{1}{Q_{cm}} dP_m + \frac{1}{Q_{cf}} dP_f$.

Referring to the Biot theory, the variation of porosity was represented using Eqs. (16) and (17). When the vibration stimulation would affect the aperture or extension of fracture, Eq. (17) was rewritten.

$$d\phi_m = \alpha_m de + \frac{dP_m}{Q_{cm}}, \tag{16}$$

$$d\phi_f = \alpha_f de + \frac{dP_f}{Q_{cf}}, \tag{17}$$

wherein $\alpha_i de$ was the porosity variation related to rock strain; $\frac{dP_m}{Q_{cm}}$ and $\frac{dP_f}{Q_{cf}}$ was the porosity variation related to the compressibility of fluid in rock matrix and crack, respectively.

The fluid viscosity was also influenced by low-frequency vibration parameters. The permeability and pseudo-threshold pressure gradient changed with the reservoir development. The related functions were referred to Zheng et al. [Zheng, Liu, Pu et al. (2016)].

(6) Definite conditions

When the low-frequency wave was excited at the injection end and expressed as a harmonic function, it was written as Eq. (18)

$$u(0,\ t) = u_0(x,t) = u_0 \exp(i\omega t), \tag{18}$$

wherein u_0 was the vibration amplitude; t was the vibration time; x was the distance from the vibration source.

A simulation was conducted in a two-dimensional physical model under constant pressure conditions as Eq. (19). The vertical seepage and its influence on wave propagation were neglected.

$$P_m(0,\ t) = P_f(0,\ t) = P_{in},\ P_m(L_{rock},\ t) = P_f(L_{rock},\ t) = P_{out}, \tag{19}$$

wherein P_{in} was the injection pressure; L_{rock} was the length of physical model; and P_{out} was the production pressure.

2.4 Governing equation group of the mathematical model

Substituting Eqs. (9), (13) to (17) into the expanded form of the continuity equations, a governing equation group of the seepage model of porous media with cracks under low frequency vibration was obtained. Defining a set of dimensionless parameters, as dimensionless displacements $u_D = u/L$, $w_{mD} = w_m/L$, $w_{fD} = w_f/L$; $x_D = x/L$; dimensionless time $t_D = \frac{k_f(\alpha_m\phi_m M_m - \alpha_f\phi_f M_f)t}{\eta L^2}$; dimensionless channeling flow rate $\lambda_{mf} = \alpha_{shape}\frac{k_m}{k_f}L^2$; elastic storativity ratio, $\omega_{mf} = \frac{\alpha_f\phi_f M_f}{\alpha_m\phi_m M_m - \alpha_f\phi_f M_f}$, $M_{mf} = \alpha_m\phi_m M_m - \alpha_f\phi_f M_f$. Then, the dimensionless matrix was derived as Eq. (20), which solved the model and was expressed by dimensionless displacements.

$$\boldsymbol{K}\frac{\partial^2 \boldsymbol{D}}{\partial t^2}+\boldsymbol{E}\frac{\partial \boldsymbol{D}}{\partial t}+\boldsymbol{F}\boldsymbol{D}=\boldsymbol{M}\nabla\nabla\cdot\boldsymbol{D}+\boldsymbol{Q} \tag{20}$$

wherein $\boldsymbol{D}=\left(u_D \quad w_{mD} \quad w_{fD}\right)^T$; the coefficient matrix was present in the appendix.

In this study, the weak form of the governing equation group Eq. (20) was first given by Eq. (21),

$$\int_\Omega\left(\boldsymbol{K}\frac{\partial^2 \boldsymbol{D}}{\partial t^2}+\boldsymbol{E}\frac{\partial \boldsymbol{D}}{\partial t}\right)\cdot\delta\boldsymbol{D}\mathrm{d}\Omega-\int_\Omega\boldsymbol{M}\nabla\nabla\cdot\boldsymbol{D}\cdot\delta\boldsymbol{D}\mathrm{d}\Omega+\int_\Omega\boldsymbol{F}\boldsymbol{D}\cdot\delta\boldsymbol{D}\mathrm{d}\Omega-\int_\Omega\boldsymbol{Q}\cdot\delta\boldsymbol{D}\mathrm{d}\Omega=0 \tag{21}$$

The standard vector-matrix notation was used and the dimensionless displacement were discretized as Eq. (22),

$$u_{Di}=\sum_{k=1}^{n_u}N_k^u\tilde{u}_{ki},\quad w_{mDi}=\sum_{k=1}^{n_w}N_k^w\tilde{w}_{ki},\quad w_{fDi}=\sum_{k=1}^{n_v}N_k^v\tilde{v}_{ki}, \tag{22}$$

wherein N_k^i is the shape function at node k; $\tilde{u}_{ki}$, $\tilde{w}_{ki}$ and $\tilde{v}_{ki}$ were the constructed vectors comprising the node values u_{Di}, w_{mDi} and w_{fDi}; n_u, n_w and n_v were the node numbers.

The equation of weak form Eq. (22) was subsequently written as Eq. (23),

$$\boldsymbol{M}\ddot{\boldsymbol{U}}+\boldsymbol{C}\dot{\boldsymbol{U}}+\boldsymbol{K}\boldsymbol{U}=\boldsymbol{F} \tag{23}$$

Wherein, $\boldsymbol{U}=\left(\tilde{u} \quad \tilde{w} \quad \tilde{v}\right)^T$, $\boldsymbol{M}=\int_\Omega\boldsymbol{B}^T\boldsymbol{K}\boldsymbol{B}\mathrm{d}\Omega\boldsymbol{U}$, $\boldsymbol{B}=\left(N_k^{\ u} \quad N_k^{\ w} \quad N_k^{\ v}\right)^T$, $\boldsymbol{C}=\int_\Omega\boldsymbol{B}^T\boldsymbol{E}\boldsymbol{B}\mathrm{d}\Omega\boldsymbol{U}$ $\boldsymbol{K}=\int_\Omega\boldsymbol{B}^T\boldsymbol{F}\boldsymbol{B}\mathrm{d}\Omega\boldsymbol{U}$, $\boldsymbol{F}=-\left(\nabla\boldsymbol{U}\right)^T\int_\Omega\boldsymbol{B}^T\boldsymbol{D}_e\boldsymbol{B}\mathrm{d}\Omega\boldsymbol{U}-\int_\Omega\boldsymbol{B}^T\boldsymbol{Q}\boldsymbol{B}\mathrm{d}\Omega\boldsymbol{U}$; $\boldsymbol{D}_e$ was a degraded matrix of $\boldsymbol{M}$.

Consider any time-dependent function to vary linearly in time between t and $t+\Delta t$, a linear algebraic system as Eq. (24) could be computed after conducting the discrete solution scheme.

$$\left[\boldsymbol{M}+\boldsymbol{C}\Delta t+\theta\boldsymbol{K}\left(\Delta t\right)^2\right]\boldsymbol{U}^{t+\Delta t}=\theta\left(\Delta t\right)^2\boldsymbol{F}^{t+\Delta t}+\left(2\boldsymbol{M}+\boldsymbol{C}\Delta t\right)\boldsymbol{U}^t-\boldsymbol{M}\boldsymbol{U}^{t-\Delta t}+\left(1-\theta\right)\cdot\left(\Delta t\right)^2\left(\boldsymbol{F}^t-\boldsymbol{K}\boldsymbol{U}^t\right), \tag{24}$$

wherein Δt was the time step; θ was a scalar value comprised between 0 and 1.

In this study, the variation of dimensionless parameters was solved with numerical method. Because the classic seepage model of dual porous media was solved with dimensionless form, it was essential to obtain dimensionless results in the study to make a comparison. Secondly, the channeling flow was related with the properties of matrix and crack. The average characteristic length of the matrix cell was hard to give a concrete value in the ideal physical model, because it was involved with crack density and crack

shape and it was usually randomly distributed in a natural formation. Then the dimensionless fluid velocity could be used to describe the average flow in a matrix cell and the values of fluid velocities could vary in a large numerical interval. Thirdly, the dimensionless solid displacement for poroelastic theory was often solved in a periodic porous medium (a minor dimensionless space, equaling the ratio of per pore length and wave length) [Yan (1999)]. Similarly, the solid displacement in this study was also solved in a minor periodic space and it was easy to reflect the wave attenuation in a matrix cell.

The matrix was solved based on the standard finite element discretization in space domain and finite difference discretization in time domain. Here the governing equation group was solved with finite element method with COMSOL Multiphysics software. Because of the complexity during the solvement of wave poroelastic problem, non-convergence and low robustness of results was often found. Researchers had made works to improve the accuracy [Ferronato, Castelletto and Gambolati (2010); Gessner (2009); Maghoul, Gatmiri and Duhamel (2011)]. Additionally, when the cracks existed in the porous media, the numerical results of fluid flow would be influenced by the crack nodes along the complicated crack paths. A great number of numerical methods had also been proposed to deal with crack problems. For example, Rabczuk et al. [Rabczuk, Zi, Bordas et al. (2010)] described a new robust and efficient approach for modeling discrete cracks in meshfree method, which was motivated by the cracking-particle method, and the crack was modeled by a set of cracked segments. A method based on local maximum entropy shape functions together with enrichment functions used in partition of unity methods was developed by Amiri et al. [Amiri, Anitescu, Arroyo et al. (2014)] to discretize problems in linear elastic fracture mechanics. Zhou et al. [Zhou, Rabczuk and Zhuang (2018)] presented the numerical implementation of the phase-field model in COMSOL, which could be essentially treated a multifield problem. Even if the crack was assumed not to propagate, but the permeability of crack would be influenced by compressibility and the simulation was involved in the coupling of multiple fields. Strategies as addition of PMLs, model size optimization, approximation order adjustment of shape functions, and proper mesh generation were introduced [Zheng and Li (2018)].

3 Numerical simulation on the wave-coupled seepage

During the process for two-dimensional simulation (Fig. 2), the direction of elastic wave propagation was set consistent with those of reservoir distribution and liquid flow at the initial time. The density, aperture, and length of micro cracks were the same as those of fractures in Chapman model so as to form uniform distributed and interconnected crack systems. Because of the assumption of high crack density and porosity, the physical properties of crack and matrix were put in a grid unit. The dimensionless fluid displacements in a crack and matrix as well as the matrix deformation were solved. Referring to the crack characteristics of X71 block in an eastern oilfield, the basic parameters of rock matrix, crack and fluid were set in Tab. 1 [Ma, Zhou and Zhao (2011)].

Table 1: Basic parameters for porous media with cracks

Basic parameters	Values	Basic parameters	Values
Vibration amplitude u_0 (μm)	100	Wave velocity in fluid V_f(m/s)	1710
Vibration frequency ω (Hz)	30	Density of matrix ρ_s (kg/cm^3)	2650
Length of model L_{rock} (m)	100	Porosity of matrix ϕ_{m0}	20%
Injection pressure P_{in} (MPa)	12	Matrix permeability k_{m0} (10^{-3} μm^2)	50
Production pressure P_{out} (MPa)	8	Porosity of crack ϕ_{f0}	0.2%
Initial pore pressure P_0 (MPa)	10	Crack permeability k_{f0} (10^{-3} μm^2)	1000
Fluid density ρ_f(kg/m^3)	1100	Radius of crack a (m)	0.1
Fluid viscosity η_0 (mPa•s)	1	Crack aperture h_{f0} (μm)	80
Volume modulus of fluid K_f(GPa)	2.25	Density of crack ε_f (m^{-1})	0.1
Modulus of rock K_s (GPa)	39.8	P wave velocity V_p^0 (km/s)	3.8
Cement content in the crack (%)	0	S wave velocity V_s^0 (km/s)	2.3

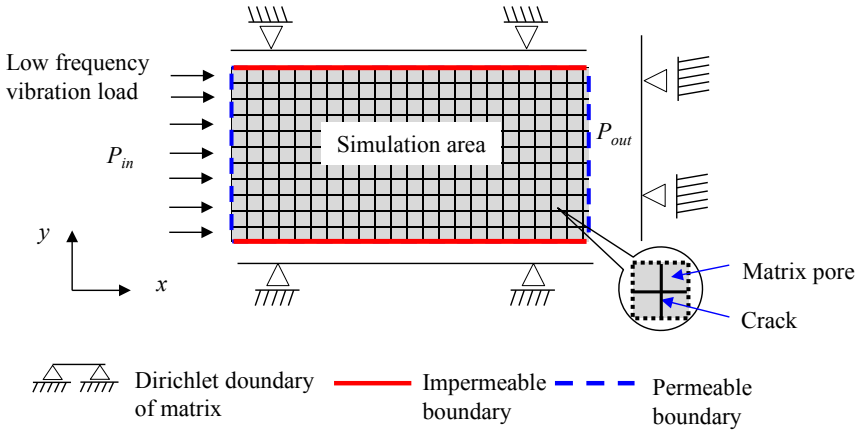

Figure 2: Physical model (virtual grids containing matrix and cracks)

(1) Dimensionless variation of physical properties in the wave-coupled seepage field

Based on the basic parameters in Tab. 1, the variation of physical properties under low-frequency vibration in porous media with cracks was solved as shown in Fig. 3. With the coupling of low-frequency wave field and flow field in dual-porous media, there was obvious deformation of rock matrix nearby the injection or production boundary. With the increase of distance from the injection boundary, the deformation of rock matrix gradually decreased and the flow velocity stabilized. The flow velocity at the boundary was much larger than in the physical model, which was apparently enhanced by wave-induced flow. As the wave propagation time increased, the solid displacement initially increased and then decreased with the attenuation of the wave. The flow velocities in the rock matrix and crack both decreased with time. The dimensionless solid

displacement u_D at the injection boundary and production boundary was, respectively, in the range of 0-1.5×10^{-6} and 0-3×10^{-7}. The dimensionless flow velocity v_{mD} and v_{fD} was in the range of 0-2×10^{-4} and 0-0.5, respectively. In terms of extents of deformation and flow velocity increase in crack, the dimensionless action distance x_D was about 0.6.

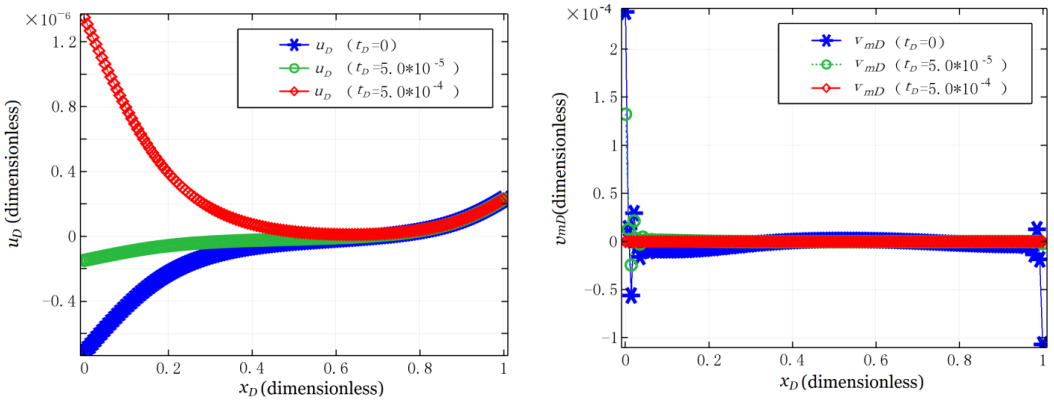

(a) Dimensionless solid phase displacement (b) dimensionless flow velocity in rock matrix

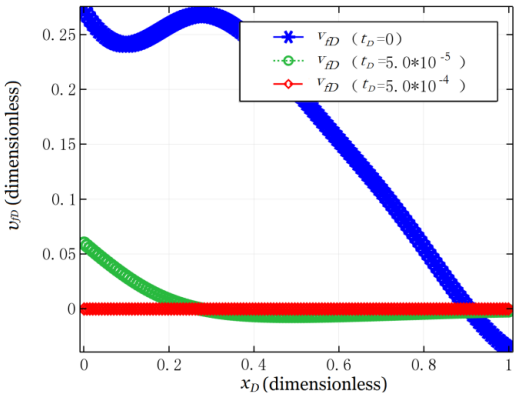

(c) dimensionless flow velocity in crack

Figure 3: Dimensionless parameters in wave coupled seepage field in rock with cracks

When the solid displacement, flow velocity, and pore pressure were expressed with actual values, they were found to periodically fluctuate with time and distance (Figs. 4 and 5). The amplitude initially increased and then decreased over time. When the wave propagation time was small, the increased flow velocity reflected that the whole conductivity of dual-porous media was enhanced by low-frequency vibration oil production technology. It was known that low-frequency vibration oil production technology was suitable for low permeability reservoirs. The wave-induced flow in the rock matrix was stronger than in cracks because of the difference of pore structures. The fluctuating pressure in rock matrix also took more time (t>0.25 s) to become stable compared to the cracks (t>0.1 s). When the simulation time was 1.0 s, the maximum pressure in the rock matrix was (13.5 MPa) was still larger than in the cracks (12.6 MPa).

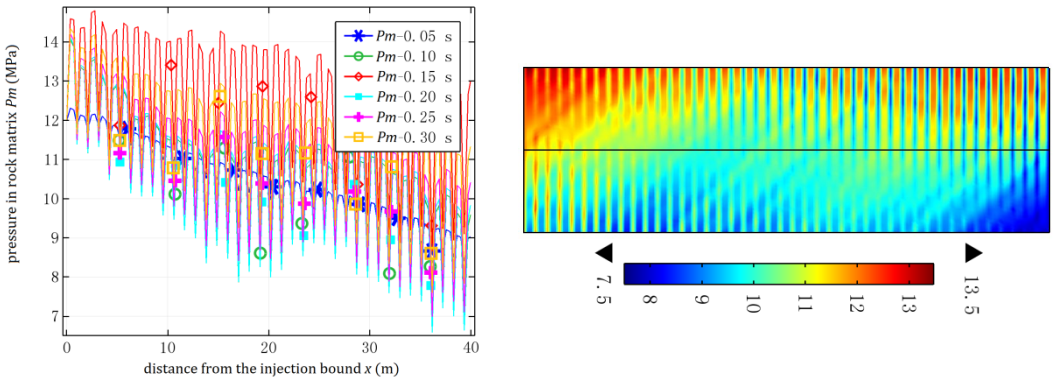

(a) Variation of pressure in rock matrix P_m (b) Distribution of P_m at t=1 s (MPa)

Figure 4: Distribution of pressures in rock matrix under low frequency vibration

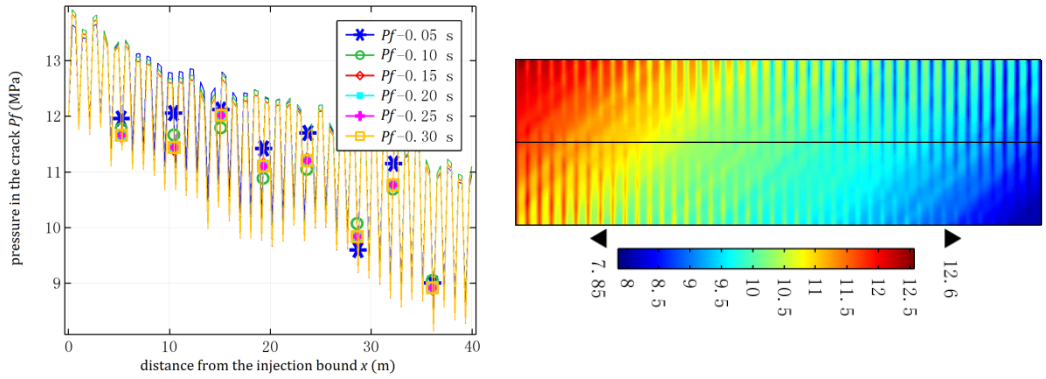

(a) Variation of pressure in crack P_f (b) Distribution of P_f at t=1 s (MPa)

Figure 5: Distribution of pressures in crack under low-frequency vibration

Simulating with the basic parameters, the channeling flow rate between rock matrix and crack under low-frequency vibration was obviously larger than that of the conventional Warren-Root seepage model. When the simulation time was large enough, the fluid velocities in rock matrix and crack in the middle of the physical model were both smaller than for the conventional Warren-Root seepage model. A stable state of seepage in the dual-porous media occurred earlier with the assistance of wave stimulation. The flow velocity in cracks was much larger than in the rock matrix, especially with the improvement of low-frequency vibration oil production technology. More fluid flowed through the cracks and the fluid displacement in the rock matrix decreased. In addition, the chosen physical model, used a virtual grid during numerical simulation of the cracks and matrix. The pressure fields of fluid in cracks and matrix were simultaneously transmitted to the downstream simulation grids through the matrix and crack. When a simulation was conducted with a different physical model, which put the information of crack and matrix in different grid, the pressure field of fluid in crack quickly transmitted to its downstream simulation grids. The pressure difference between matrix and crack

was enlarged. The fluid velocity in the crack and the channeling flow rate was, respectively, larger than in the Warren-Root model. Certainly, the flow velocity in the rock matrix was still smaller than that of the conventional Warren-Root model when the simulation time was large.

(2) Comparison with a case assuming non-existence of pressure difference at the initial time

For the studies in petrophysics, the fluid was usually assumed static (or non-existence of pressure difference) at the initial time. The fluid in dual-porous media moved under the excitation of low-frequency vibration. This case only considered the effect of wave-induced flow, which was different for this study. A comparison with a case assuming non-existence of pressure difference at the initial time was done (Fig. 6). It was found that the simulations considering the initial flow or not would get different results. When assuming non-existence of pressure difference at the initial time, the wave-induced flow velocity in rock matrix and crack was, respectively, only in the range of 0.4-2.0 μm /s and 1.0-3.0 mm/s at t=0-0.3 s. The simulated pressure in rock matrix and crack was in the range of 2-15 MPa and 10-11 MPa at t=0-0.3 s, respectively. The fluid nearby the injection or production boundary moved towards the vibration source, while the fluid inside the rock moved in the opposite direction. Because the wave-induced inertial effect in the rock matrix was larger than in the crack in the area nearby the injection or production boundary, the channeling flow was from the matrix to the crack. The largest value of flow velocity in the rock matrix in this case was one-third of that in wave-coupled seepage field, in which there existed a pressure difference at the initial time. However, in terms of the wave-induced effect, the fluctuating extent of physical properties in this case was a little stronger than that in wave-coupled seepage field, because the latter was influenced by the inertial effect of fluid flow at the initial time.

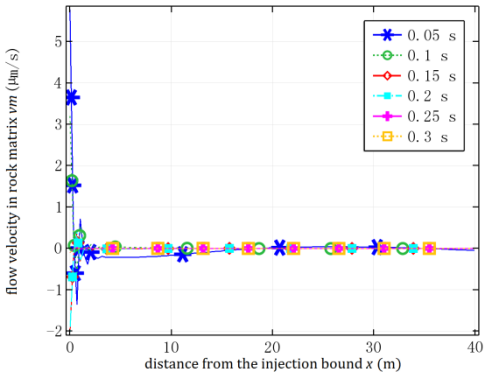

(a) flow velocity in matrix with initial flow

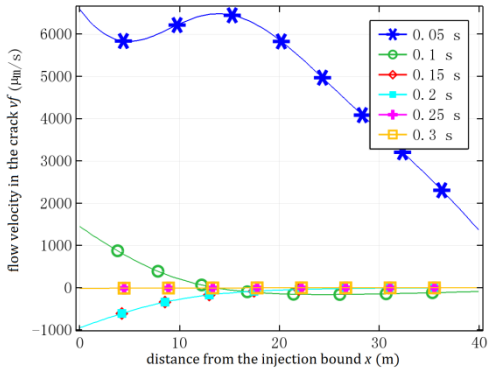

(b) flow velocity in crack with initial flow

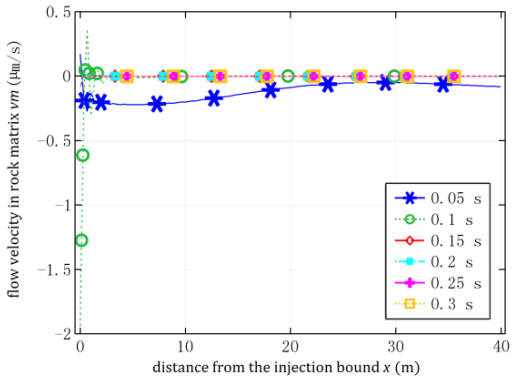

(c) flow velocity in matrix without initial flow

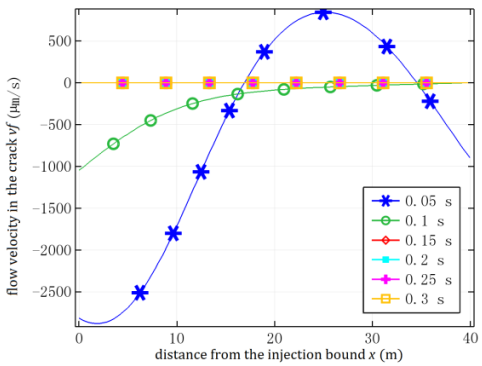

(d) flow velocity in crack without initial flow

Figure 6: Comparison on the flow velocities of fluid in crack and rock matrix considering initial flow or not

The simulation results showed that the enhanced flow by low-frequency vibration oil production technology was weakened in a porous media with multiple pore structures, in comparison to the stimulation effect in a porous media with a single-pore structure. This technology still played a positive role in overcoming the threshold pressure gradient, plug removal in pore-throat, and energy supplement. In a field trial, a strong shock on the downhole wellbore was sustained, instead of imposing a short, attenuated wave. The whole conductivity and channeling flow rate between the matrix and crack might be improved under certain vibration parameters.

4 Sensitive analyses on the variation of dimensionless parameters

A parametric study was conducted to investigate the influence of vibration parameters and heterogeneity on the dimensionless parameters in a wave-coupled seepage field. Here, the heterogeneity was expressed by the ratio of crack permeability to matrix permeability [Yang, Tham, Tang et al. (2004)]. The variation of the maximum value of dimensionless parameters (defined as Eq. (25)) in a certain vibration period was analyzed in the parametric study. The vibration period was chosen one second in this paper when the seepage field became already stable.

$$\max\left(\overline{\overline{\Re}}\right)=\max\left\{\text{average}\left(\Re\right)\Big|_{\Omega},t\le 1\text{s}\right\} \tag{25}$$

wherein $\Re$ was the parameters in wave-coupled seepage field, like dimensionless flow velocities of fluid in crack and rock matrix, dimensionless pressure of rock matrix, and channeling flow rate.

(1) Influence of vibration frequency

Within a given range of vibration frequency values, the dimensionless parameters had repeatedly decreased and increased (Figs. 7-9). The sensitivity analysis about frequency showed that there existed several natural frequencies. Different dimensionless parameters

corresponded to various optimal vibration frequencies. In the range of vibration frequency, the parameters of wave-coupled seepage flow repeatedly decrease and increase, but the optimal vibration frequency is different for various parameters. The dimensionless flow velocity in matrix v_{mD} reached the maximum value when the vibration frequency was close to 70-80 Hz, while the dimensionless flow velocity in crack v_{fD} reached the maximum value at about 50-80 Hz. The dimensionless pressure in the matrix and the channeling flow rate both had larger values at higher vibration frequency. The optimal frequency for dimensionless flow velocity was generally opposite to that for dimensionless pressure in matrix.

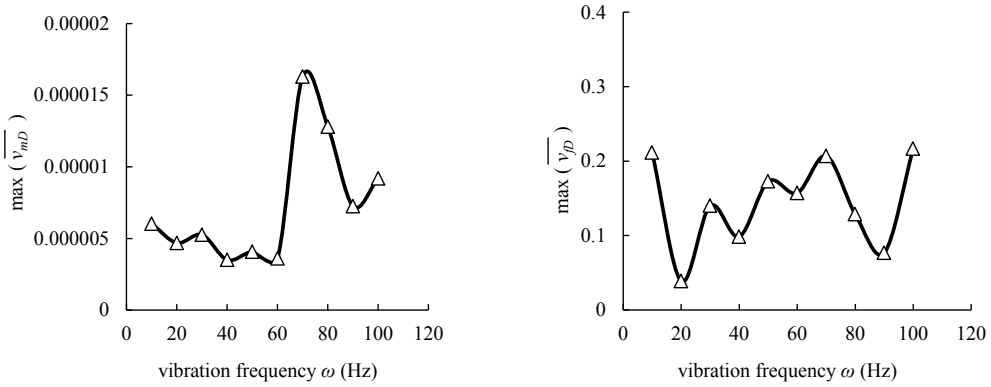

(a) dimensionless flow velocity in matrix (b) dimensionless flow velocity in crack

Figure 7: Influence of vibration frequency on dimensionless flow velocity

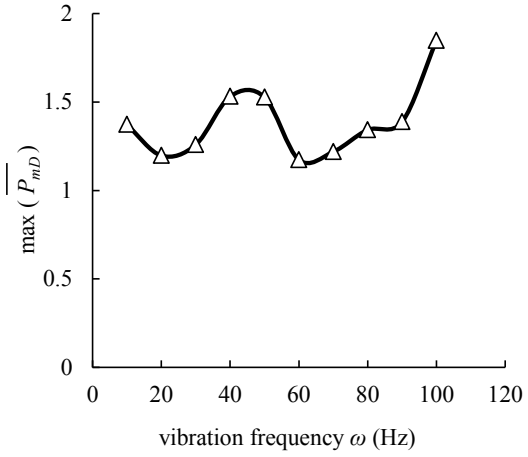

Figure 8: Influence of vibration frequency on dimensionless pressure in matrix

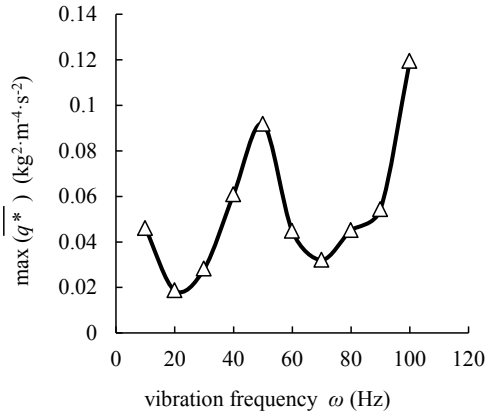

Figure 9: Influence of vibration frequency on channeling flow rate q^*

Compared with the sensitivity rule about vibration frequency in a porous media of only matrix pores, the variation of dimensionless parameters of dual porous media was small because of the weakened stimulation effect. In the case of only matrix pores, the flow velocity nearby the injection boundary increased with vibration frequency. The local optimal frequency for flow velocity was generally the same as that for pore pressure in matrix. The trend of dimensionless parameters versus frequency was obvious different. It might be improper to explain the mechanism of low frequency vibration oil production technology in dual porous media, by blindly following the rules in porous media with single pore structure.

When the producing degree of fluid in matrix was to improve in a heterogeneous fractured low permeability reservoir, an appropriate vibration frequency should be optimized. The vibration frequency was usually close to the natural frequency of matrix. When the channeling flow was to enhance in such situation as imbibition, plugging removal with the matrix being polluted, and matrix acidification [Yang, Li, Tao et al. (2018)], it was suggested to increase the vibration frequency as much as possible.

(2) Influence of vibration amplitude

With the increase of vibration amplitude, the dimensionless flow velocity and pressure in rock matrix as well as the channeling flow rate had generally increased, while the dimensionless flow velocity in the crack had repeatedly decreased and then increased (Figs. 10-12). Local optimal amplitude could still be chosen to make a relatively large improvement in conductivity and channeling.

With the assumed physical model in Fig. 2, the pressure field could transmit to its downstream simulating grid because the crack network had a high conductivity. The wave-induced inertial effect would initially increase and be imposed on the rock matrix, when the vibration amplitude became larger. The effective stress on the rock was decreased. The porosity and permeability of the rock matrix was slightly improved, considering the stress sensitivity in a low permeability formation. Correspondingly, fluid flow in the matrix was enhanced and the flow in the crack was relatively reduced. The pressure difference between the crack and rock matrix as well as the channeling flow would also be increased.

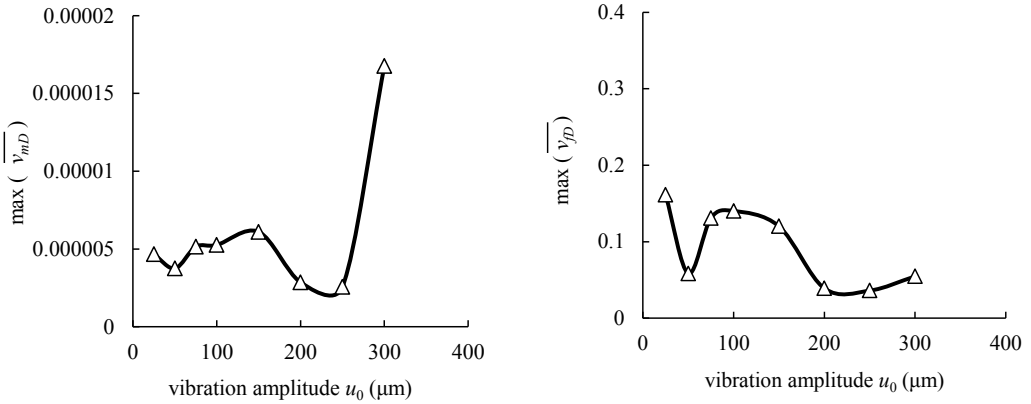

(a) dimensionless flow velocity in matrix (b) dimensionless flow velocity in crack

Figure 10: Influence of vibration frequency on dimensionless flow velocity

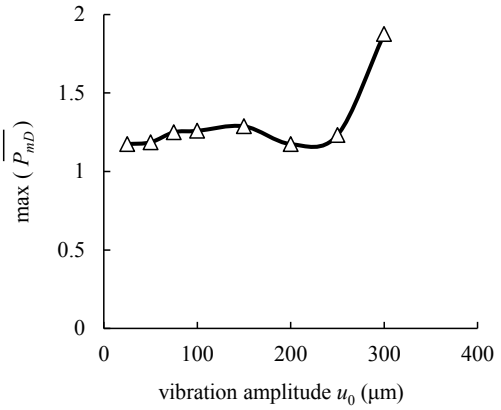

Figure 11: Influence of vibration frequency on dimensionless pressure in matrix

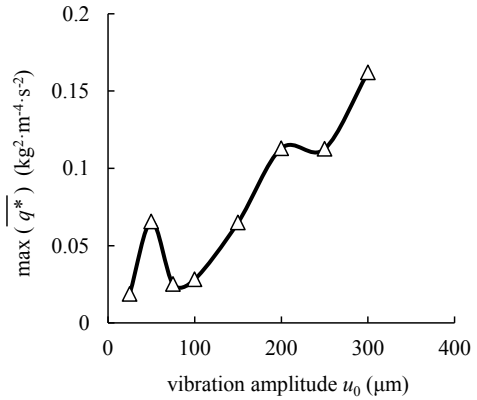

Figure 12: Influence of vibration frequency on channeling flow rate q^*

The sensitivity rule about vibration amplitude in dual porous media was similar to that in a porous media with single pore structure. The results showed that when the cracks were interconnected and of high density, the device power should be enhanced as much as possible to increase the downhole vibration amplitude in field trial [Zheng, Pu and Liu (2018)]. However, additional simulation with low density cracks or isolated cracks had demonstrated that the optimal vibration amplitude should be chosen. The optimal amplitude was suggested 50 μm or 150 μm to enhance the fluid flow in rock matrix; and 100 μm was suggested to increase the channeling flow rate between crack and rock matrix.

(3) Influence of crack-matrix permeability ratio

The influence of crack-matrix permeability ratio on physical properties of wave-coupled seepage field of porous media is shown in Figs. 13-14. When the ratio of crack permeability to matrix permeability was kept constant, the dimensionless flow velocity and pressure in the rock matrix decreased linearly as the rock permeability increased. A repeating pattern of increase and then decrease was found with the channeling flow rate.

When the permeability of rock matrix kept constant and the crack-matrix permeability ratio increased, it was equivalent to the case of keeping the crack permeability constant and reducing permeability of rock matrix. The value of crack-matrix permeability ratio had been positive correlated with the micro heterogeneity. The dimensionless flow velocity in rock matrix in the wave coupled seepage field had decreased with the heterogeneity increasing. The channeling flow rate had varied with an unapparent rule. For the results in Fig. 13, the channeling flow generally decrease firstly and then increased when the crack-matrix permeability ratio was 10, 20 and 30. Three cycles of a trend of increase firstly and then decrease had been found with the channeling flow when the crack-matrix permeability ratio was 15 and 25.

On one hand, the results showed that the variation of dimensionless flow velocity followed a similar rule when the dual-porous media had the same micro heterogeneity. The similar distribution of pressure field at the initial time would reduce the contribution to the wave-coupled seepage field. However, the crack permeability had a great influence on the physical properties of wave-coupled seepage field. The inertial effect of initial flow on wave-coupled seepage was weakened, when the permeability of rock matrix as well as the crack-matrix permeability ratio both increased. Under the condition of similar crack-matrix permeability ratio, low-frequency vibration oil production technology was suggested to apply in an area with lower permeability. The producing degree of fluid in the matrix would increase, although channeling flow would be slightly reduced. This would be useful to avoid pollution in matrix pores and increase conductivity of whole rock.

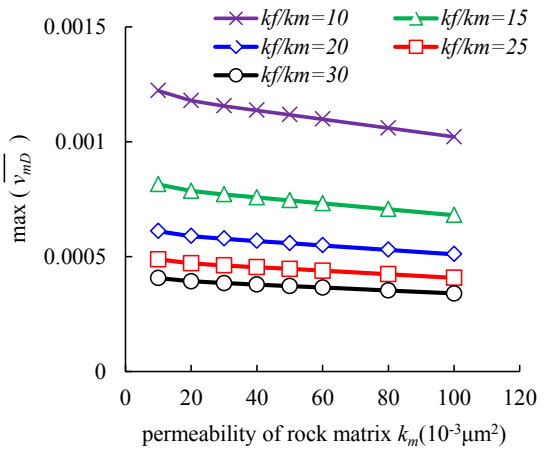

Figure 13: Influence of vibration frequency on dimensionless flow velocity in matrix v_{mD}

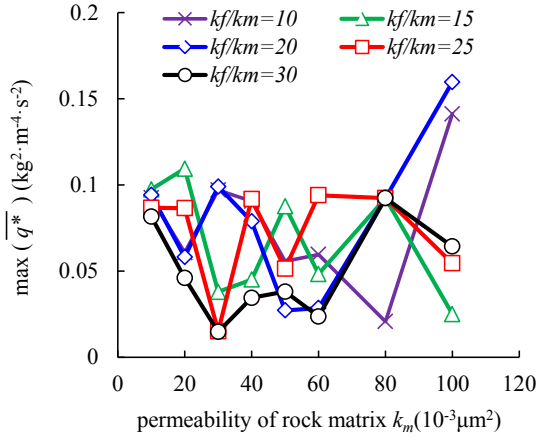

Figure 14: Influence of vibration frequency on channeling flow rate q^*

5 Conclusions

(1) A model of seepage in porous media with cracks under low-frequency vibration was obtained by combining the wave propagation theory in fractured porous media and seepage mechanics of dual-porous media. It was useful to explain the mechanism of low-frequency wave stimulation technology in developing reservoirs. The constitution of the Chapman model and the continuity equation of the Warren-Root model were coupled for a case assuming high crack density in this study. The dimensionless matrix for solving the model was given.

(2) The existence of cracks might weaken the stimulation effect of wave-induced flow in the rock matrix. The channeling flow between the rock matrix and crack could be enhanced by the imposed low-frequency vibration. The sensitive analyses indicated that there were differences between the rule about variation of wave-coupled seepage field in dual-porous media and in porous media with single-pore structure. Simulated with the

parameters in Tab. 1, when the vibration frequency was about 70-80 Hz, and the amplitude was 50 μm or 150 μm, more improvement of dimensionless flow velocity in rock matrix was observed. When the vibration frequency was close to 50 Hz or 100 Hz and the amplitude was large enough, the channeling flow increased to a greater degree. Different vibration parameters were needed to achieve better improvement of the fluid velocity in the rock matrix or to further increase the channeling flow rate.

(3) Similar to the solution of poroelastic theory, the numerical results were found to be seriously influenced by the physical parameters and mesh generation method. Irregular curve and fluctuation of data were got in the sensitive analyses. A study on the convergence and robustness of results was needed to improve the mechanism. Considering that the real low permeable reservoir was saturated with multiple phase fluid and usually hydraulic fractured, a simulation on the multiple phase flow under wave stimulation was necessary, with crack propagation simultaneously.

Acknowledgement: The authors would like to thank the Scientific and Technological Research Project of Higher Education Institutions in Hebei Province (QN2019163), China Postdoctoral Science Foundation (2018M631765), the Doctoral Funds of Yanshan University (BL17024) and a grant from Hebei Province Postdoctoral Advanced Programs (B2018003011).

Conflicts of Interest: The authors declare that they have no conflicts of interest to report regarding the present study.

References

Alexandre, S.; Philip, M. B.; Ben, D. T.; Jim, F. H.; Paul, Y. (2006): Quantifying damage, saturation and anisotropy in cracked rocks by inverting elastic wave velocities. *Pure and Applied Geophysics*, vol. 163, no. 5-6, pp. 947-973.

Amiri, F.; Anitescu, C.; Arroyo, M.; Bordas, S. P. A.; Rabczuk, T. (2014): XLME interpolants, a seamless bridge between XFEM and enriched meshless methods. *Computational Mechanics*, vol. 53, no.1, pp. 45-57.

Berryman, J. G. (1979): Theory of elastic properties of composite-materials. *Applied Physics Letters*, vol. 35, no. 11, pp. 856-858.

Berryman, J. G. (2007): Seismic waves in rocks with fluids and fractures. *Geophysical Journal International*, vol. 171, no. 2, pp. 954-974.

Biot, M. A. (1956): Theory of propagation of elastic waves in a fluid-saturated porous solid. I. Low-frequency range. *Journal of the Acoustical Society of America*, vol. 28, no. 2, pp. 168-178.

Chapman, M. (2003): Frequency-dependent anisotropy due to mesoscale fractures in the presence of equant porosity. *Geophysical Prospecting*, vol. 51, no. 5, pp. 369-379.

Chapman, M. (2009): Modeling the effect of multiple fracture sets of mesoscale fractures in porous rock on frequency-dependent anisotropy. *Geophysics*, vol. 74, no. 6, pp. 97-103.

Corapcioglu, M. Y. (1973): Fundamentals of transport phenomena in porous media. *Engineering Geology*, vol. 7, no. 2, pp. 169-170.

Dusseault, M.; Davidson, B.; Spanos, T. (2000): Pressure pulsing: the ups and downs of starting a new technology. *Journal of Canadian Petroleum Technology*, vol. 39, no. 4, pp. 13-17.

Dvorkin, J.; Mavko, G.; Nur, A. (1995): Squirt flow in fully saturated rocks. *Geophysics*, vol. 60, no. 1, pp. 97-107.

Ekanem, A. M.; Li, X. Y.; Chapman, M.; Ian, M.; Wei, J. X. (2014): Effect of fracture aperture on p-wave attenuation: a seismic physical modelling study. *ISRN Geophysics*, vol. 2014, pp. 1-8.

Ferronato, M.; Castelletto, N.; Gambolati, G. (2010): A fully coupled 3-D mixed finite element model of Biot consolidation. *Journal of Computational Physics*, vol. 229, no. 12, pp. 4813-4830.

Gessner, K. (2009): Coupled models of Brittle-plastic deformation and fluid flow: approaches, methods, and application to mesoproterozoic mineralisation at mount Isa, Australia. *Surveys in Geophysics*, vol. 30, no. 3, pp. 211-232.

Fang, X. J.; Jin, F. (2007): Coupling model for interaction between fissure water and cracking in concrete. *Shuili Xuebao*, vol. 38, no. 12, pp. 1466-1474.

He, P.; Xiong, J. Y.; Lu, Z. H.; Pan, L. H.; Qin, D. W. (2018): Study of pulse wave propagation and attenuation mechanism in shale reservoirs during pulse hydraulic fracturing. *Arabian Journal for Science and Engineering*, vol. 43, no. 11, pp. 6509-6522.

Hudson, J. A.; Pointer, T.; Liu, E. (2001): Effective-medium theories for fluid-saturated materials with aligned cracks. *Geophysical Prospecting*, vol. 49, no. 5, pp. 509-522.

Karve, P. M.; Kallivokas, L. F.; Manuel, L. (2017): A framework for assessing the uncertainty in wave energy delivery to targeted subsurface formations. *Journal of Applied Geophysics*, vol. 125, pp. 26-36.

Lei, P. (2014): *Experimental Testing Theory and Equipment Development for Interporosity Flow Coefficient in Fractured- Porous Dual Media (Ph.D. Thesis)*. Southwest Petroleum University, Chengdu.

Ma, S. Q. (2019). Research on coal seam permeability improvement by high-voltage electric pulse discharge. *Safety in Coal Mines*, vol. 50, no. 5, pp. 15-18.

Ma, Z. G.; Zhou, F.; Zhao, Q. (2011): Elastic properties of tight sands in the lower Shihezi formation of Ordos basin. *Acta Petrolei Sinica*, vol. 32, no. 6, pp. 1001-1006.

Maghoul, P.; Gatmiri, B.; Duhamel, D. (2011): Wave propagation in unsaturated poroelastic media: boundary integral formulation and three-dimensional fundamental solution. *Computer Modeling in Engineering & Sciences*, vol. 78, no. 1, pp. 51-75.

Mavko, G.; Mukerji, T.; Dvorkin, J. (1998): *The Rock Physics Handbook: Tools for Seismic Analysis in Porous Media*. Cambridge University Press, New York.

Mosaheb, M.; Zeidouni, M.; Shakiba, M. (2018): Pressure pulse testing method for caprock characterization. *SPE Annual Technical Conference and Exhibition*, pp. 24-26.

Ning, J.; Ning, S. N.; Shi, Y. L.; Duan, J. B. (2004): Some methods for making

fractures and increasing permeability of porous media by means of two_shockwave interference technique. *Acta Petrolei Sinica*, vol. 25, no. 3, pp. 79-82, 90.

Pu, C. S.; Zheng, L. M.; Liu, J. (2017): Innovations and challenges of vibration coupled seepage mechanics in oil and gas reservoir development. *Earth Science*, vol. 42, no. 8, pp. 1247-1262.

Rabczuk, T.; Zi, G.; Bordas, S.; Nguyen-Xuan, H. (2010): A simple and robust three-dimensional cracking-particle method without enrichment. *Computer Methods in Applied Mechanics and Engineering*, vol. 199, no. 37-40, pp. 2437-2455.

Saiood, H.; Duthie, L.; Shaheen, S.; Albaqshi, A.; Ali, M. (2018): Newly designed flow activated pulsation tool for coiled tubing deployed matrix acidizing stimulation applications in extended reach carbonate reservoirs. *Abu Dhabi International Petroleum Exhibition & Conference*, 12-15 November, Abu Dhabi, UAE.

Tian, S. C.; Huang, Z. W.; Li, G. S.; Lu, P. Q.; Zhang, H. Y. et al. (2018): Laboratory experiments on blockage removing and stimulation of CBM reservoirs by composite pulsating fracturing of radial horizontal wells. *Natural Gas Industry*, vol. 38, no. 9, pp. 88-94.

Vladimir, G. (2014): Seismic characterization of fractured reservoirs. *SEG Encyclopedia of Exploration Geophysics*, pp. 1-12.

Wang, J. C.; Xie, W.; Gao, F.; Xie, X. Q. (2016) Experimental study and application of low frequency vibration profile control by air foam. *Unconventonal Oil & Gas*, vol. 3, no. 5, pp. 83-87.

Wang, W. Q.; Rutqvist, J.; Görke, U. J.; Birkholzer, J. T.; Kolditz, O. (2011): Non-isothermal flow in low permeable porous media: a comparison of Richards' and two-phase flow approaches. *Environmental Earth Sciences*, vol. 62, no. 6, pp. 1197-1207.

Warren, J. E.; Root, P. J. (1963): The behavior of naturally fractured reservoirs. *Society of Petroleum Engineers Journal*, vol. 3, no. 3, pp. 245-255.

Wu, J.; Zhang, S. H.; Cao, H.; Kemeny, J. (2016): The effect of pulse frequency on the acoustic emission characteristics in coal bed hydraulic fracturing. *50th U.S. Rock Mechanics/Geomechanics Symposium*.

Yan, P. (1999): *Reservoir Analysis Using Intermediate Frequency Excitation (Ph.D. Thesis)*, pp. 11-17. Stanford University.

Yang, Q. L.; Li, L. B.; Tao, S. Y.; Lu, X. B.; Zhu, J. Y. (2018): Chelate acid pulse injection and acidizing stimulation technology for immobilized injecting well string. *Petroleum Drilling Techniques*, vol. 46, no. 5, pp. 90-94.

Yang, T. H.; Tham, L. G.; Tang, C. A.; Liang, Z. Z.; Tsui, Y. (2004): Influence of heterogeneity of mechanical properties on hydraulic fracturing in permeable rocks. *Rock Mechanics and Rock Engineering*, vol. 37, no. 4, pp. 251-275.

Zhang, H. Y.; Huang, Z. W.; Li, G. S.; Lu, P. Q.; Tian, S. C. et al. (2018): Fracture propagation laws and acoustic emission response characteristics of coal radial well-pulse hydraulic fracturing. *Acta Petrolei Sinica*, vol. 39, no. 4, pp. 472-481.

Zhang, P. (2011): *A Study on Artificial Earthquake Oil Recovery Disturbance System and Technology (Ph. D. Thesis)*. Xi'an Shiyou University, Xi'an.

Zheng, L. M.; Li, Z. F. (2018): Numerical analysis of simulation accuracy for seepage change in one-dimensional layer under low-frequency wave. *Geotechnical and Geological Engineering*, vol. 36, no. 1, pp. 497-519.

Zheng, L. M.; Liu, J.; Pu, C. S.; Xu, J. X; Li, Y. J. (2016): Seepage analysis under low-frequency vibration in one-dimensional porous media model saturated with single-phase percolating fluid. *Chinese Journal of Rock Mechanics and Engineering*, vol. 35, no. 10, pp. 2098-2105.

Zheng, L. M.; Pu, C. S.; Liu, J. (2018): Influence of low-frequency vibration oil recovery on the initial flow of radial reservoir. *Petroleum Geology and Recovery Efficiency*, vol. 25, no. 1, pp. 68-76.

Zhou, S. W.; Rabczuk, T.; Zhuang, X. Y. (2018): Phase field modeling of quasi-static and dynamic crack propagation: COMSOL implementation and case studies. *Advances in Engineering Software*, vol. 122, pp. 31-49.

Appendix A

The coefficient matrix of Eq. (20) was as follows.

$$\boldsymbol{K}=\begin{bmatrix} \dfrac{k_f^{\,2}M_{mf}^{\,2}}{\eta^2L^2}\left(\dfrac{\rho}{M_{mf}}-\dfrac{\rho_m\Re_m}{M_m}\right) & \dfrac{k_f^{\,2}\rho_m}{\eta^2L^2}\left(M_{mf}-\dfrac{\Re_m M_{mf}^{\,2}}{\phi_m M_m}\right) & 0 \\ \dfrac{\Re_m\rho_m k_f^{\,2}M_{mf}^{\,2}}{M_m\eta^2L^2} & \dfrac{\Re_m\rho_m k_f^{\,2}M_{mf}^{\,2}}{\phi_m M_m\eta^2L^2} & 0 \\ \left(\dfrac{\Re_m\rho_m}{M_m}+\dfrac{\rho_f}{M_f}\right)\dfrac{k_f^{\,2}M_{mf}^{\,2}}{\eta^2L^2} & \dfrac{\Re_m\rho_m k_f^{\,2}M_{mf}^{\,2}}{\phi_m M_m\eta^2L^2} & \dfrac{\rho_f k_f^{\,2}M_{mf}^{\,2}}{\phi_f M_f\eta^2L^2} \end{bmatrix},$$

$$\boldsymbol{E}=\begin{bmatrix} 0 & -\dfrac{k_f\alpha_m\phi_m\left(1+2\omega_{mf}\right)\Re_m}{k_m\left(1+\omega_{mf}\right)} & 0 \\ \dfrac{\lambda_{mf}k_f^{\,2}\left(\Re_m\rho_m-\rho_f\right)M_{mf}}{\eta^2L^2} & \left(\dfrac{\Re_m}{M_m k_m}+\dfrac{\lambda_{mf}k_f\Re_m\rho_m}{\phi_m\eta^2L^2}\right)k_f M_{mf} & -\dfrac{\lambda_{mf}\rho_f k_f^{\,2}M_{mf}}{\phi_f\eta^2L^2} \\ 0 & \dfrac{\Re_m k_f\alpha_m\phi_m\left(1+2\omega_{mf}\right)}{k_m\left(1+\omega_{mf}\right)} & \dfrac{\alpha_f\phi_f}{\omega_{mf}} \end{bmatrix},$$

$$\boldsymbol{F}=\begin{bmatrix}0 & 0 & 0\\ 0 & \dfrac{\lambda_{mf}k_f}{k_m}\Re_m & -\lambda_{mf}\\ 0 & 0 & 0\end{bmatrix},\quad \boldsymbol{M}=\begin{bmatrix}\omega_{mf}\left(\dfrac{C}{\alpha_f\phi_f M_f}+\alpha\right) & \omega_{mf} & \omega_{mf}\\ \alpha_m+\phi_m & 1 & 0\\ \alpha & 1 & 1\end{bmatrix},$$

$$\boldsymbol{Q}=\begin{bmatrix}\left(\dfrac{\rho_s b^S}{M_{mf}}-\dfrac{\lambda_0+\rho_m {b_m}^F}{M_m}\right)L\\ \int\dfrac{\alpha_{shape}k_m\left(\lambda_0+\rho_m b^F-\rho_f b^F\right)L^3}{k_f M_{mf}}dt_D\\ \left(\dfrac{1}{M_m}\rho_m b^F+\dfrac{1}{M_f}\rho_f b^F+\dfrac{1}{M_m}\lambda_0\right)L+\nabla\left(\int\dfrac{q_0\eta L^3}{\rho_f k_f M_{mf}}dt_D\right)\end{bmatrix}.$$

Among them, $\dfrac{1}{M_i}=\dfrac{\phi_i}{K_f}+\dfrac{1}{Q_{ci}}$, $\Re_m=1-\dfrac{2J_1\left(\lambda_m R_m\right)}{\lambda_m R_m J_0\left(\lambda_m R_m\right)}$.